DELPHI Collaboration

DELPHI 2004-022-CONF-697
20 July, 2004

Study of Tau-pair Production in Photon-Photon Collisions at LEP and Limits on the Anomalous Electromagnetic Moments of the Tau Lepton

I.Boyko, V.Zhuravlov
Joint Institute for Nuclear Research

Abstract

Tau-pair production in the process $e^+e^- \to e^+e^-\tau^+\tau^-$ was studied using data collected by the DELPHI experiment at LEP2 during the years 1997 – 2000. The corresponding integrated luminosity is 650 pb^{-1}. The values of the cross-section obtained are found to be in agreement with QED predictions. Limits on the anomalous magnetic and electric dipole moments of the tau lepton are deduced.

Contributed Paper for ICHEP 2004 (Beijing)

1 Introduction

This paper presents a study of tau pair production in photon-photon collisions using the data collected by the DELPHI detector at LEP in the period from 1997 to 2000 (LEP2) at collision energy $\sqrt{s}$ between 183 and 208 GeV. The total integrated luminosity used in the analysis is 650 pb^{-1}. At LEP this process was first observed by the OPAL collaboration [1] and subsequently studied by the L3 collaboration [2].

The final state $e^+e^-\tau^+\tau^-$ can be produced via a set of Feynman diagrams. In this paper we present the cross-section measurement for the contribution of the so-called multiperipheral graph (Fig. 1) which corresponds to collisions of two virtual photons. The same final states produced via other diagrams (less then 1% of the cross-section) are considered as a background.

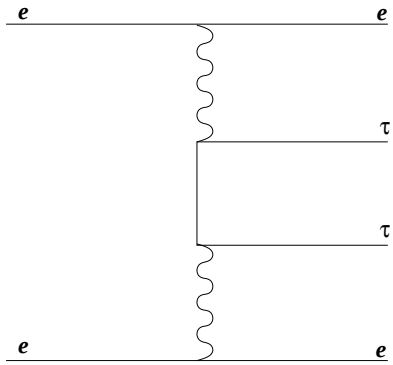

Figure 1: The dominant diagram for the reaction $e^+e^- \to e^+e^-\tau^+\tau^-$

The study of the reaction $e^+e^- \to e^+e^-\tau^+\tau^-$ explores two fundamental problems. First of all it provides a deep test of QED at the level of the fourth order in α. Furthermore, the $\gamma\tau\tau$ vertex is sensitive to the anomalous electromagnetic couplings of the tau lepton. Since the multiperipheral $e^+e^- \to e^+e^-\tau^+\tau^-$ process diagram contains two such vertices, the anomalous magnetic and electric dipole moments can be extracted by comparing the measured cross-section with QED expectations.

The rest of the paper gives a detailed description of the $e^+e^- \to e^+e^-\tau^+\tau^-$ cross-section measurement, including tau-pair selection, background estimation, selection and trigger efficiency calculation and systematic error estimation. In the last part of the paper the measured cross-sections are used to derive limits on the anomalous electromagnetic moments of the tau lepton.

2 Monte Carlo simulation

The signal process was simulated using the Berends, Daverveldt and Kleiss generator RADCOR (BDKRC) [3], which calculates the cross-section for the multiperipheral diagram with radiative corrections on the electron and positron lines. The following signal definition was used: the invariant mass of tau pairs had to be less than 40 GeV/c^2; both beam particles had to be scattered by less than 10 degrees; and at least one of them had to be scattered by less than 2 degrees. With these restrictions the accepted cross-section was 1.44±0.04% lower than the total cross-section predicted by BDKRC (which is about

450 pb at LEP2 energies) for the unrestricted phase space. The τ decay was simulated by the TAUOLA package [4], which includes photon radiation from the decay products. The BDKRC generator was also used to estimate the background coming from the process $e^+e^- \to e^+e^-\mu^+\mu^-$.

To simulate the $e^+e^- \to e^+e^-e^+e^-$ background, the Berends, Daverveldt and Kleiss generator DIAG36 (BDK) [5] was used. Hadron production in two photon collisions was simulated by PYTHIA 6.1 [6]. Non-multiperipheral four-fermion processes (such as WW, ZZ, Zee and others) were simulated by WPHACT [7].

The generated events were passed through the full simulation program of the DELPHI detector and were reconstructed with the same program as for the real data [8].

3 Event selection

In most events produced by two-photon collisions both beam particles scatter at small angles and remain undetectable inside the beam pipe. Therefore only the decay products of the tau leptons can be seen in the detector. To suppress background, only one-prong decay channels with one tau decaying into an electron and the other into a non-electron (hadron or muon) were considered. The analysis was based entirely on the measured tracks of charged products of tau decays; the neutral particles from tau decays were ignored in this analysis.

To select runs with good performance of the sub-detectors [8]–[9], only runs with the Time Projection Chamber (TPC), the Forward Chambers (FCA, FCB) and one of the additional barrel tracking detectors (ID or VD) fully operational were retained. Table 1 presents the luminosities used in the analysis, luminosity-weighted centre-of-mass energies and energy ranges.

	1997	1998	1999	2000
Luminosity, pb^{-1}	52.3	152.6	224.2	217.5
$< E_{cm} >$, GeV	182.7	188.7	197.6	206.3
Energy range, GeV	182.7	188.7	195.5 – 201.5	204.5 – 208.0

Table 1: The integrated luminosities, mean collision energies and collision energy ranges.

The event selection procedure was divided into two steps. The first step (preselection) selected a sample of two-photon events with two good tracks which were not back-to-back in the plane perpendicular to the beam axis. A track was considered as good if the momentum derived from its curvature was greater than 100 MeV/c, momentum error better than 100%, polar angle θ between 20° and 160°, and impact parameter with respect to the interaction point below 10 cm along the z-axis [1] and 5 cm in the $r - \phi$ plane.

The following cuts were applied in this first selection step:

- There had to be exactly two good tracks from particles with opposite charges, at least one of them having momentum greater than 300 MeV/c.

[1] The DELPHI coordinate system has the z-axis aligned along the electron beam direction, the x-axis pointing toward the centre of LEP and the y-axis vertical. r is the radius in the (x, y) plane. The polar angle θ is measured with respect to the z-axis and the azimuthal angle ϕ is about z.

- To suppress background from fermion pair production, the total energy of two charged particles had to be less than 30 GeV.

- To enrich the sample with $e^+e^- \to e^+e^-\tau^+\tau^-$ events, the acoplanarity of two tracks [2] had to be greater than 0.5° and their resultant transverse momentum greater than 500 MeV/c.

- To select events with a high trigger efficiency, the transverse energy, defined by

$$E_t = E_1 \sin\theta_1 + E_2 \sin\theta_2,$$

  where E_1 and E_2 are the energies of the two charged particles and θ_1 and θ_2 are their polar angles, had to be greater than 2 GeV.

- In the year 2000, the operation of one of the twelve TPC sectors was unstable and the *dE/dx* measurement vital for this analysis was poor, so events with at least one track in or near (closer than 10° in ϕ) to this TPC sector in 2000 were rejected.

- Finally, to ensure the transverse momentum balance of $\gamma\gamma$ system, single and double tagged events were rejected by requiring that no energy deposition in the forward electromagnetic calorimeters (STIC or FEMC) exceeded 60% of the beam energy.

The last cut suppressed the events with highly virtual photons. About 90% of events passing this cut had the momentum transfer $-q^2$ less then 1 GeV$^2/c^2$. After applying the cuts described above, the predicted event composition in the preselected sample was as follows (1999 data):

$e^+e^- \to e^+e^-e^+e^-$	41 %
$e^+e^- \to e^+e^-\mu^+\mu^-$	47 %
$e^+e^- \to e^+e^-\tau^+\tau^-$	8 %
$e^+e^- \to e^+e^-q\bar{q}$	3 %
$e^+e^- \to \tau^+\tau^-$	1 %

The fraction of other events was less than 1%. The efficiency of the preselection for $e^+e^- \to e^+e^-\tau^+\tau^-$ events was of the order of 5%, the largest suppression of the signal coming from the requirement of exactly two good tracks seen in the detector (about a factor of 4) and from the cut on E_t (about factor of 2). Figure 2 shows the comparison between data and simulation of the distributions of invariant mass, total energy, total transverse energy and total transverse momentum of the pair of charged particles. The $e^+e^- \to e^+e^-\tau^+\tau^-$ events are shown by the shaded histogram. The Monte Carlo is normalised to the luminosity of the real data. The data deficit is mainly due to the trigger inefficiency which is corrected at the later stages of analysis.

In the final step of the selection, the event was retained if one of the charged particles was identified as an electron and the other as a non-electron. This step was based on the TPC measurement of the *dE/dx* pulls for the muon, electron, kaon and proton hypotheses. The *dE/dx* pull for a specific particle hypothesis is defined as the ratio

$$\Pi_X = \frac{(\mathrm{d}E/\mathrm{d}x)_{meas} - (\mathrm{d}E/\mathrm{d}x)_{exp}}{\sigma_{\mathrm{d}E/\mathrm{d}x}}, \qquad (1)$$

[2] Acoplanarity is defined as $180° - |\phi_2 - \phi_1|$.

where $(\mathrm{d}E/\mathrm{d}x)_{exp}$ is the value expected for the particle X with given momentum and $\sigma_{\mathrm{d}E/\mathrm{d}x}$ is the error of the measured energy loss $(\mathrm{d}E/\mathrm{d}x)_{meas}$. To check the *dE/dx* calibration, test samples of $\mathrm{e}^+e^- \to e^+e^-\mu^+\mu^-$ and $\mathrm{e}^+e^- \to e^+e^-e^+e^-$ events were picked out from the preselected sample. A small angular dependence of the *dE/dx* measurements was found as well as some disagreement between data and simulation. Corrections which were functions of azimuthal and polar angle were applied to the measured *dE/dx* values. Residual disagreement was removed by scaling and smearing the specific energy loss measurement in the simulated events. Independent calibrations of real and simulated data were performed for each year of data taking analysed. The efficiency to measure *dE/dx* is discussed later in the paper.

With corrected *dE/dx* information, a track was identified as an electron if $\Pi_\mu > 3$ and as a non-electron if $\Pi_\mathrm{e} < -3$. Figure 3 illustrates the particle identification cuts. The distributions of the pulls for the electron and muon hypotheses are shown for the 1999 real data and simulation. Each distribution is shown after applying all selection cuts except the cut on the variable shown. The shaded histograms show the signal.

A considerable amount of kaon and proton background from $\mathrm{e}^+e^- \to e^+e^-q\bar{q}$ events remained after the cuts on the pulls for the muon and electron hypotheses. Figure 4 (left) shows the specific energy loss for electron candidates plotted versus the momentum of the particle. Proton and kaon bands are clearly visible. To remove the kaon and proton background, the electron selection was tightened. The *dE/dx* for the electron candidate had to not exceed 1.9 times the minimum ionisation, and the pulls for the proton and kaon hypotheses for the electron candidate both had to be outside the $\pm 1.5\sigma$ interval: $|\Pi_\mathrm{K}| > 1.5$ and $|\Pi_\mathrm{p}| > 1.5$. Figure 4 (right) shows the distribution of the pull for the proton hypothesis with all selection cuts applied except the cut on the variable shown. The hatched histogram shows the background from $\mathrm{e}^+e^- \to e^+e^-q\bar{q}$ events, the shaded histogram shows the rest of the background. The cuts on this variable are indicated by arrows.

Table 2 summarises the efficiency of the preselection, final step of selection and overall selection efficiency. The drop in the preselection in 2000 is caused by the removal of events in or near the unstable TPC sector. The uncertainties of the selection efficiency determination are discussed later in the paper.

	1997	1998	1999	2000
preselection	5.39	5.37	5.38	3.85
selection	17.3	16.4	16.4	16.1
overall	0.93	0.88	0.88	0.62

Table 2: Efficiencies (%): preselection, final step of selection and overall efficiency.

In total 2390 candidate events were selected. Figure 5 compares the distributions of electron and non-electron candidate momenta for selected events to the simulation prediction for the combined 1997-2000 data. Figure 6 shows the visible invariant mass distribution for selected events for the same data sample. Trigger efficiency is taken into account in these distributions (see below).

3.1 Trigger efficiency

The low momenta of the τ decay products in the process $e^+e^- \to e^+e^-\tau^+\tau^-$ and the presence of only two tracks in the event could make the probability of triggering on such an event considerably below 100%. The determination of the trigger efficiency is therefore important in this analysis.

The trigger efficiency was estimated from the subsamples of selected events using the fact that an event can be detected by different components of the DELPHI trigger system [10]. Trigger subcomponents of the tracking system were combined into barrel and end-cap triggers. For events with one track in the barrel and the other in the end-cap, the number of events detected by the barrel trigger (N_B), by the end-cap trigger (N_E), and by both triggers (N_{BE}) were counted using the decision functions of the trigger. The barrel and end-cap single track trigger efficiencies were calculated, for electrons and non-electrons separately, by the formulae:

$$\varepsilon_{Barrel} = \frac{N_{BE}}{N_E}; \qquad \varepsilon_{end-cap} = \frac{N_{BE}}{N_B}. \tag{2}$$

Finally, the efficiency of the DELPHI calorimetric trigger to the whole event was estimated from the events triggered by any of the tracking detectors using a similar technique. The results of the trigger efficiency calculation are summarised in Table 3. The track pair trigger efficiency was calculated from the "OR" of the single track efficiencies using the ratio of the barrel and forward tracks predicted by simulation. The tau pair trigger efficiency was calculated as "OR" of the tracking and calorimetric triggers.

		1997	1998	1999	2000
Barrel track					
	electron	71.4 ± 17.1	94.4 ± 5.4	84.6 ± 7.1	92.3 ± 7.4
	non-electron	$100^{+0}_{-17.9}$	85.2 ± 6.8	85.0 ± 8.0	78.6 ± 11.0
End-cap track					
	electron	26.3 ± 10.1	36.5 ± 6.1	21.5 ± 4.6	22.0 ± 6.9
	non-electron	31.3 ± 11.6	30.4 ± 6.1	25.9 ± 4.8	23.1 ± 5.8
Track pair		$94.5^{+5.5}_{-7.1}$	95.5 ± 2.7	93.3 ± 3.5	93.5 ± 4.1
Calorimetry		6.7 ± 1.9	8.6 ± 1.2	7.1 ± 0.9	7.7 ± 1.1
Tau pair		$94.9^{+5.1}_{-6.6}$	95.9 ± 2.5	93.8 ± 3.3	94.0 ± 3.8

Table 3: Summary of the trigger efficiency measurements (%)

3.2 Efficiency of the *dE/dx* measurement

Both tracks of the selected event had to have specific energy loss measurements. An imperfect detector simulation can lead to a discrepancy in the *dE/dx* measurement efficiency for good tracks in real and simulated events. To take into account this possible disagreement, the efficiency for a good track to have a *dE/dx* measurement (to be a "good TPC track") was calculated for $e^+e^- \to e^+e^-e^+e^-$ and $e^+e^- \to e^+e^-\mu^+\mu^-$ samples extracted from preselected events (efficiencies to measure *dE/dx* of pions and muons were assumed to be equal). Muon events were selected by requiring at least one track to be identified by

the muon chambers and electron events were selected using information from the DELPHI RICH detectors. For muon and electron events the efficiency to be a "good TPC track" was determined from the ratio

$$\varepsilon^2_{\mathrm{d}E/\mathrm{d}x} = \frac{N_{\mathrm{d}E/\mathrm{d}x}}{N_{tot}} \tag{3}$$

where $N_{\mathrm{d}E/\mathrm{d}x}$ is the number of events with both tracks having a *dE/dx* measurement and N_{tot} was the total number of selected events in the given sample. The tau-pair efficiency was estimated as the product of the single track efficiencies for muon and electron. The tau-pair efficiencies derived from $\mathrm{e}^+e^- \to e^+e^-\mu^+\mu^-$ and $\mathrm{e}^+e^- \to e^+e^-e^+e^-$ events for data and Monte Carlo are presented in Table 4 and were used for selection efficiency correction and for systematic error estimation. The selection efficiency was multiplied by the factor $\frac{\varepsilon_{\mathrm{d}E/\mathrm{d}x}(data)}{\varepsilon_{\mathrm{d}E/\mathrm{d}x}(MC)}$ and half of the correction was included into the systematic error together with the uncertainties from the test sample statistics.

	1997	1998	1999	2000
Efficiency in data, %	82.9 ± 1.0	82.6 ± 0.6	82.4 ± 0.5	83.5 ± 0.6
Efficiency in MC, %	82.3 ± 0.4	82.5 ± 0.2	82.3 ± 0.1	84.6 ± 0.2

Table 4: Summary of "good TPC track" efficiency estimations. These efficiencies are already included in the total efficiency in Table 2.

3.3 Residual background

Several sources of background for $e^+e^- \to e^+e^-\tau^+\tau^-$ events have been considered:

- The background from $\mathrm{e}^+e^- \to e^+e^-q\bar{q}$, mainly from protons and kaons selected due to the tails of the *dE/dx* pulls for the proton and kaon hypotheses;
- The background from $\mathrm{e}^+e^- \to e^+e^-e^+e^-$ and $\mathrm{e}^+e^- \to e^+e^-\mu^+\mu^-$ events due to the tails of the distributions of the *dE/dx* pulls for the electron and muon hypotheses;
- Background due to other four-fermion processes: non-multiperipheral diagrams (including $\mathrm{e}^+e^-\tau^+\tau^-$ final states) and multiperipheral process $e^+e^- \to e^+e^-\tau^+\tau^-$ which does not satisfy signal definition;
- The process $\mathrm{e}^+e^- \to \tau^+\tau^-$ (background from other fermion pair production processes was found to be negligible).

The background fractions for the main background sources and their uncertainties are summarised in Table 5. The contribution from other background sources was negligible. The theoretical precision of $\mathrm{e}^+e^- \to e^+e^-q\bar{q}$ generation by PYTHIA is not well known. Therefore it was estimated from the real data by inverting the *dE/dx* cut on the electron candidate: *dE/dx* >1.9 M.I.P. instead of *dE/dx* <1.9 M.I.P. After comparing these test samples enriched with $\mathrm{e}^+e^- \to e^+e^-q\bar{q}$ events with the simulation, an error of 20% was ascribed to the $\mathrm{e}^+e^- \to e^+e^-q\bar{q}$ event generator.

Channel	1997	1998	1999	2000
$e^+e^- \to e^+e^-q\bar{q}$	4.3 ± 1.5	3.2 ± 0.7	3.3 ± 0.8	3.2 ± 0.8
$e^+e^- \to e^+e^-e^+e^-$	2.7 ± 0.2	3.4 ± 0.1	4.0 ± 0.1	2.4 ± 0.1
$e^+e^- \to e^+e^-\mu\mu$	2.9 ± 0.1	5.0 ± 0.1	2.4 ± 0.1	3.8 ± 0.1
other 4-fermion	1.5 ± 0.3	1.5 ± 0.3	1.2 ± 0.2	1.2 ± 0.2
$e^+e^- \to \tau\tau$	0.69 ± 0.01	0.55 ± 0.01	0.47 ± 0.01	0.40 ± 0.01
Total	12.1 ± 1.5	13.6 ± 0.8	11.4 ± 0.8	11.0 ± 0.8

Table 5: Summary of background fractions. The numbers are the expected fractions (%) of the specified backgrounds in the selected sample. Errors are statistical errors of the simulated samples and theoretical uncertainties of the Monte Carlo generators added in quadrature.

4 Systematic error estimation

The following sources of systematic error on the cross-section measurement were considered: uncertainties of selection and trigger efficiencies and uncertainty of background level. Track selection, event selection and the statistical error of the simulated samples were taken into account in the calculation of the uncertainty in the selection efficiency.

The systematic error arising from track selection was estimated in the following way. Each cut of the track selection was varied typically by the size of the resolution of the corresponding variable from its nominal value in both directions. The corresponding change of the cross-section Δ was compared to the value of the expected statistical fluctuation σ due to the non-identical event sample. If the value Δ was less than σ, no systematic error was ascribed to the corresponding cut; in the opposite case the value of $\sqrt{\Delta^2 - \sigma^2}$ was included in the systematic error. The systematic error arising from varying the event selection cuts was estimated in a similar way.

To calculate the systematic error due to the angular corrections applied to the *dE/dx* measurements, the *dE/dx* correction functions were varied by the uncertainty of each of their parameters and the analysis chain was repeated. The variation of the measured cross-section was added to the systematic error. The systematic errors corresponding to scaling and smearing the pulls were calculated similarly.

The systematic errors associated with track selection cuts, event selection cuts and *dE/dx* corrections are summarised in Table 6. The numbers are given for 1999 data (for other years uncertainties of most of the sources scale approximately as inverse square root of the statistics). Additional contributions to the selection efficiency uncertainty also presented in Table 6 come from the statistical error of the Monte Carlo sample and the selection efficiency correction described in Section 3.2.

The largest contribution to the systematic error is given by the uncertainty of the trigger efficiency determination, dominated by the statistics of the real data events, see Section 3.1 and Table 3. An additional contribution arises because the trigger efficiency for background events, assumed to be equal to that of the signal, may be different. A conservative estimate of this uncertainty was obtained by changing the trigger efficiency for background upwards to 100% and downwards by the same amount.

The systematic error due to residual background includes the simulated sample statistical uncertainty and the theoretical uncertainty of the Monte Carlo generators, mainly

syst. error source		value, %
track selection cuts		
	R_{imp}	0.7
	Z_{imp}	1.1
	$\delta p/p$	0.7
event selection cuts		
	Π_{e}	0.3
	Π_{μ}	0.3
	acoplanarity	0.6
dE/dx corrections		
	Π_{e} θ	1.0
	Π_{e} ϕ	0.9
	Π_{μ} θ	1.0
	Π_{μ} ϕ	1.0
	scaling	0.7
	smearing	0.6
MC statistics		0.8
"Good TPC track" correction		0.6
Total		3.0

Table 6: Systematic errors for 1999 data coming from track selection, event selection, *dE/dx* corrections, simulated samples statistics and "good TPC track" correction.

for the $\mathrm{e}^+e^- \to e^+e^-q\bar{q}$ process, see Table 5.

The sources of selection efficiency uncertainty are described in detail in Table 6.

The sources of systematic uncertainty are summarised in Table 7. Total systematic errors calculated as the sum in quadrature of all described components are also presented in Table 7. The following uncertainties were assumed to be fully correlated between different years: generator theoretical error; trigger efficiency for background; and uncertainties estimated from variation of track and event selection cuts. Systematic errors from other sources were treated as uncorrelated.

	1997	1998	1999	2000
Trigger eff.	7.0	2.7	3.6	4.5
Selection eff.	5.1	3.2	3.0	3.0
Background	1.7	0.9	0.9	0.9
Luminosity	0.6	0.6	0.6	0.6
Total	8.9	4.3	4.7	5.4

Table 7: Relative systematic errors on cross-section (in %).

5 Results of the cross-section measurement

The cross-sections were computed using the formula

$$\sigma = \frac{N_{obs} - N_{bg}}{\varepsilon_{sel}\varepsilon_{trig}\mathcal{L}} \tag{4}$$

where N_{obs} is the number of observed events, N_{bg} is the expected number of background events in the assumption that background events have the same trigger efficiency as signal events, ε_{sel} is the selection efficiency, ε_{trig} is the trigger efficiency and $\mathcal{L}$ is the integrated luminosity.

The numbers of observed and expected events, the measured cross-sections and the cross-sections from the BDKRC Monte Carlo simulation together with their ratios are presented in Table 8. The predicted number of events was calculated from the signal and background simulation, taking into account trigger efficiency and corrections to the *dE/dx* efficiency. Agreement was found between the measurements and the Standard Model (SM) predictions calculated by BDKRC. The ratio of observed and predicted cross-sections was averaged over all LEP2 data, taking into account correlations of systematic errors. The result was found to be 0.96 ± 0.04. The average LEP2 cross-section is 429 ± 17 pb corresponding to the luminosity-weighted mean centre-of-mass energy of 197.1 GeV. The cross-section predicted at this energy by BDKRC is 447.7 ± 0.3 pb.

Year	Observed	Expected	σ_{meas}, pb	σ_{MC}, pb	$\sigma_{meas}/\sigma_{MC}$
1997	211	224 ± 18	$401 \pm 32 \pm 36$	428.2 ± 0.5	0.94 ± 0.11
1998	629	652 ± 24	$419 \pm 19 \pm 18$	436.7 ± 0.5	0.96 ± 0.06
1999	909	937 ± 39	$436 \pm 16 \pm 21$	448.5 ± 0.5	0.97 ± 0.06
2000	641	665 ± 32	$443 \pm 20 \pm 24$	459.4 ± 0.5	0.97 ± 0.07

Table 8: The numbers of observed and expected events, measured cross-sections, QED predictions and their ratios. The first error on the measured cross-sections is statistical, the second is systematic.

6 Determination of anomalous magnetic and electric dipole moments

In the Standard Model, leptons are considered as point-like objects. Therefore the observation of a deviation of the magnetic or electric dipole moments of the leptons from their SM values would open a window onto the physics beyond the SM. The anomalous magnetic moments of the electron [11] and muon [12] are known with high precision, but the short life-time of the tau-lepton does not allow measurement of its anomalous moments with similar precision by a spin precession method.

The generalised form of the $\tau\tau\gamma$ vertex can be parametrised as follows:

$$-ie\bar{u}(p')\{F_1(q^2)\gamma^\mu + iF_2(q^2)\sigma^{\mu\nu}\frac{q_\nu}{2m_\tau} + F_3(q^2)\gamma^5\sigma^{\mu\nu}\frac{q_\nu}{2m_\tau}\}u(p)\epsilon_\mu(q) \tag{5}$$

where $\epsilon_\mu(q)$ is the polarization vector of the photon with momentum q. The form factor F_1 describes the distribution of electric charge and $e_\tau = eF_1(0)$, while F_2 and F_3 are form factors related to the anomalous magnetic moment a_τ and electric dipole moment d_τ:

$$a_\tau \equiv \frac{g_\tau - 2}{2} = F_2(0) \tag{6}$$

and

$$F_3(0) = -\frac{2m_\tau d_\tau}{e_\tau} \tag{7}$$

In the SM at tree level, $a_\tau = 0$ and $d_\tau = 0$. Accounting for loop diagrams gives a non-zero value to $a_\tau = 11773(3) \cdot 10^{-7}$ [13], while a non-zero value of d_τ is forbidden by both T invariance and P invariance.

The values of a_τ and d_τ have been measured by several groups. The L3 and OPAL collaborations [14, 15] studied radiative $Z \to \tau\tau\gamma$ events and set the following 95 % CL limits on the values of the anomalous magnetic and electric dipole moments:

$$\begin{array}{lll} -0.052 < a_\tau < 0.058 & \text{and } |d_\tau| < 3.1 \ \ (10^{-16}\ e \cdot \text{cm}) & \text{(L3)} \\ -0.068 < a_\tau < 0.065 & \text{and } |d_\tau| < 3.7 \ \ (10^{-16}\ e \cdot \text{cm}) & \text{(OPAL).} \end{array}$$

The best limit so far on d_τ was obtained by BELLE [16]:

$$-0.22 < \Re e(d_\tau) < 0.45 \ \ (10^{-16} e \cdot \text{cm})$$
$$-0.25 < \Im m(d_\tau) < 0.08 \ \ (10^{-16} e \cdot \text{cm})$$

Other limits on a_τ and d_τ can be found in [17].

6.1 Limits from this analysis

Here we present the study of the anomalous magnetic and electric dipole moments of the tau lepton based on the analysis of the $e^+e^- \to e^+e^-\tau^+\tau^-$ cross-section. The study of anomalous couplings of tau leptons to photons at LEP in this channel was proposed in [18].

To model the contribution of non-SM anomalous magnetic and dipole moments we use the calculation by Cornet and Illana [19]. The calculation is based on computation of the matrix element of the process $\gamma\gamma \to \tau^+\tau^-$ in leading order of QED and its translation to the cross-section of the $e^+e^- \to e^+e^-\tau^+\tau^-$ process using the Equivalent Photon Approximation (EPA) [20]. The EPA parameter $(-q^2)_{max}$ (the upper limit of the integration over 4-momenta of the emitted photon) was chosen such that the total cross-section predicted by EPA (with SM values of anomalous electromagnetic moments) agreed with BDKRC calculation. According to the calculations [19] each of the anomalous terms of (5) would mainly modify the rate of tau pair production in the barrel region of the detector where the experimental selection has largest efficiency. This leads to a larger selection efficiency for the anomalous term contribution, improving in principle the limits obtained on anomalous moments. However in this paper we conservatively assumed that the standard and anomalous contributions have the same selection efficiency.

Figure 7 shows how the total cross-section changes as a function of the anomalous magnetic moment and as a function of the electric dipole moment. The three lines on each plot represent the calculation with $\sqrt{s}$ =182.7, 195.5 and 205.0 GeV. Increasing

the collision energy slowly increases both non-SM contributions. However, increasing the magnitude of the anomalous magnetic moment can either increase or decrease the cross-section while increasing that of the electric dipole moment tends only to increase the cross-section.

To compare the experimentally measured values of the cross-sections to the non-SM calculation, they were first converted from accepted to the total cross-sections, taking into account the 1.44% difference due to the signal definition (see section 2). The validity of applying SM conversion factors is supported by the fact that the measured cross-sections are in good agreement with the SM prediction, which guarantees the smallness of the non-SM contribution, and by the fact that the correction itself is small.

Fits to the cross-sections measured in 1997, 1998, 1999 and 2000 were performed taking a_τ and d_τ as parameters. When fitting for a_τ, the value of d_τ was set to its SM value and *vice versa*. The errors on the cross section measurements were taken as the statistical and systematic errors added in quadrature.

To quote the obtained limits we used the following convention:

$$\int_{-\infty}^{L} \exp\left(-\chi^2/2\right) da_\tau = \int_{R}^{\infty} \exp\left(-\chi^2/2\right) da_\tau = \frac{1-CL}{2} \tag{8}$$

where CL is the desired confidence level and L and R are lower and upper limits. A similar definition was used for d_τ. We quote central values μ and errors σ for moments according to

$$\sigma = \frac{R-L}{2}, \quad \mu = \frac{R+L}{2}. \tag{9}$$

where R and L are calculated with 68.3% confidence level.

Figure 8 shows the χ^2 as a function of the anomalous magnetic moment and as a function of the electric dipole moment. The results of the fit are:

$$\begin{array}{ll} -0.052 < a_\tau < 0.013, & 95\%\ \text{CL} \\ |d_\tau| < 3.7 \cdot 10^{-16}\ e \cdot \text{cm}, & 95\%\ \text{CL}. \end{array}$$

The limit on a_τ improves the current PDG limit [21] based on the L3 result [14].

Figure 9 shows the the measured cross-section, average LEP2 cross-section and SM expectation as a function of $\sqrt{s}$. Two bands superimposed on the plot represent the allowed region for the cross-section variation due to anomalous magnetic and electric dipole moments. The results expressed in the form of central value and error are the following:

$$\begin{array}{c} a_\tau = -0.018 \pm 0.017, \\ d_\tau = (0.0 \pm 2.0) \cdot 10^{-16}\ e \cdot \text{cm}. \end{array}$$

7 Conclusion

We have studied the reaction $e^+e^- \to e^+e^-\tau^+\tau^-$ with the data collected with the DELPHI detector during LEP2 operation in the years 1997-2000. The average LEP2 cross-section was found to be 429±17 pb compared to 447.7 pb expected from the Standard model. The measured/predicted ratio 0.96±0.04 agrees with the QED prediction at the

level of one standard deviation. The measured cross-sections were used to extract limits on the anomalous magnetic and electric dipole moments of the tau lepton. The 95% CL limits obtained are

$$-0.052 < a_\tau < 0.013$$
$$|d_\tau| < 3.7 \cdot 10^{-16}\ e \cdot \text{cm}.$$

Acknowledgements

We thank F.Cornet for providing the calculation of the cross-section of anomalous tau-pair production in two-photon collisions.

References

[1] OPAL Collaboration, R. Akers *et al.,* Zeit. Phys. **C60** (1993) 593.

[2] L3 Collaboration, M. Acciarri *et al.,* Phys. Lett. **B407** (1997) 341.

[3] F.A. Berends, P.H. Daverveldt, R. Kleiss, Comp. Phys. Comm. **40** (1986) 271.

[4] S. Jadach, J. Kühn, Z. Wąs, Comp. Phys. Comm. **64** (1991) 275.

[5] F.A. Berends, P.H. Daverveldt, R. Kleiss, Comp. Phys. Comm. **40** (1986) 285.

[6] T. Sjöstrand *et al.,* Comp. Phys. Comm. **135** (2001) 228.

[7] E. Accomando and A. Ballestrero, Comp. Phys. Comm. **99** (1997) 270;
E. Accomando, A. Ballestrero and E. Maina, Comp. Phys. Comm. **150** (2003) 166.

[8] DELPHI Collaboration, P. Abreu *et al.,* Nucl. Instr. and Meth. **A378** (1996) 57.

[9] DELPHI Collaboration, P. Aarnio *et al.,* Nucl. Instr. and Meth. **A303** (1991) 233;

[10] A. Augustinus *et al., The DELPHI Trigger System at LEP2 Energies*, CERN-EP/2002-086, Accepted by Nucl. Instr. and Meth. A.

[11] P.J. Mohr, B.N. Taylor, J. Phys. Chem. Ref. Data **28** (1999) 1713;
P.J. Mohr, B.N. Taylor, Rev. Mod. Phys. **72** (2000) 351.

[12] Muon g-2 Collaboration, G.W. Bennett *et al.,* Phys. Rev. Lett. **89** (2002) 101804.

[13] M.A. Samuel, G. Li, R. Mendel, Phys. Rev. Lett. **67** (1991) 668; *erratum ibid.* **69** (1992) 995.

[14] L3 Collaboration, M. Acciarri *et al.,* Phys. Lett. **B434** (1998) 169.

[15] OPAL Collaboration, K. Ackerstaff *et al.,* Phys. Lett. **B431** (1998) 188.

[16] BELLE Collaboration, K. Inami *et al.,* Phys. Lett. **B551** (2003) 16.

[17] G.A. Gonzalez-Sprinberg, A. Santamaria and J.Vidal, Nucl. Phys. **B582** (2000) 3.
R. Escribano, E. Massó, Phys. Lett. **B395** (1997) 369.
D.J. Silverman, G.L. Shaw, Phys. Rev. **D27** (1983) 1196.
F. del Aguila, M. Sher, Phys. Lett. **B252** (1990) 116.
ARGUS Collaboration, H. Albrecht *et al.,* Phys. Lett. **B485** (2000) 37.

[18] F. Cornet and J. Illana, Phys. Rev. **D53** (1996) 1181.

[19] F. Cornet, private communication,
J. Illana, *"Estudio de las propiedades electromagneticas del boson W y del lepton tau en procesos de dos fotones"*, doctoral thesis (*in Spanish*), University of Granada, (1995).

[20] V.M. Budnev *et al.,* Phys. Rep. **15** (1975) 181.

[21] K. Hagiwara *et al.,* Phys. Rev. **D66** (2002) 010001.

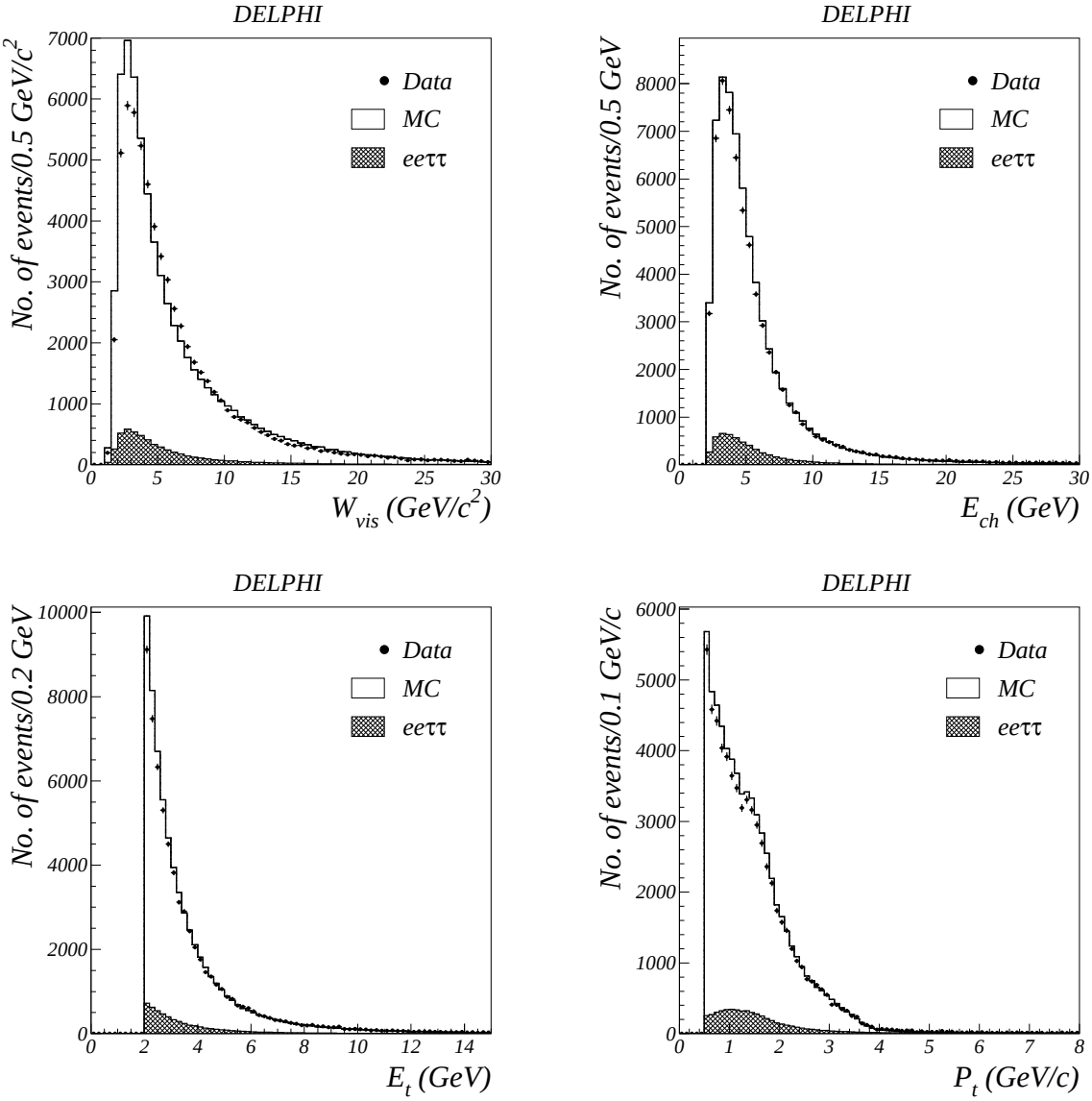

Figure 2: The distributions of invariant mass, total energy, transverse energy and transverse momentum of the pair of charged particles. Preselection cuts are applied. The points are 1999 data, the open histogram is the simulation of background processes and the shaded histogram is the simulation of $e^+e^- \to e^+e^-\tau^+\tau^-$ events. The simulation is not corrected for the trigger efficiency.

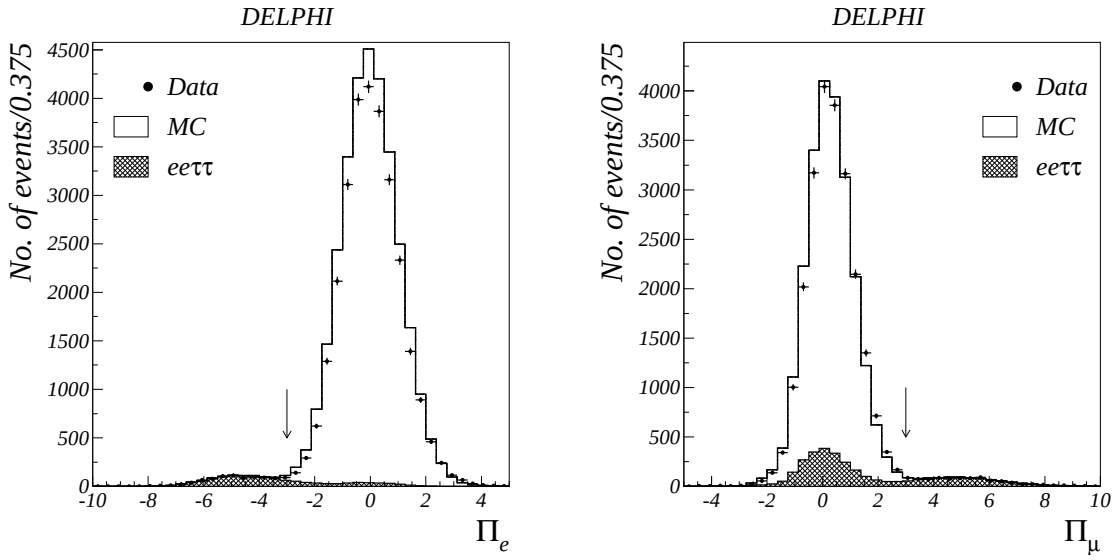

Figure 3: Distribution of the *dE/dx* pull for the electron hypothesis (left) and for the muon hypothesis (right) with all selection cuts applied except the cut on the variable shown. Points are 1999 data, the open histogram is the background, and the shaded histogram shows the $e^+e^- \to e^+e^-\tau^+\tau^-$ signal events. The simulation is not corrected for the trigger efficiency.

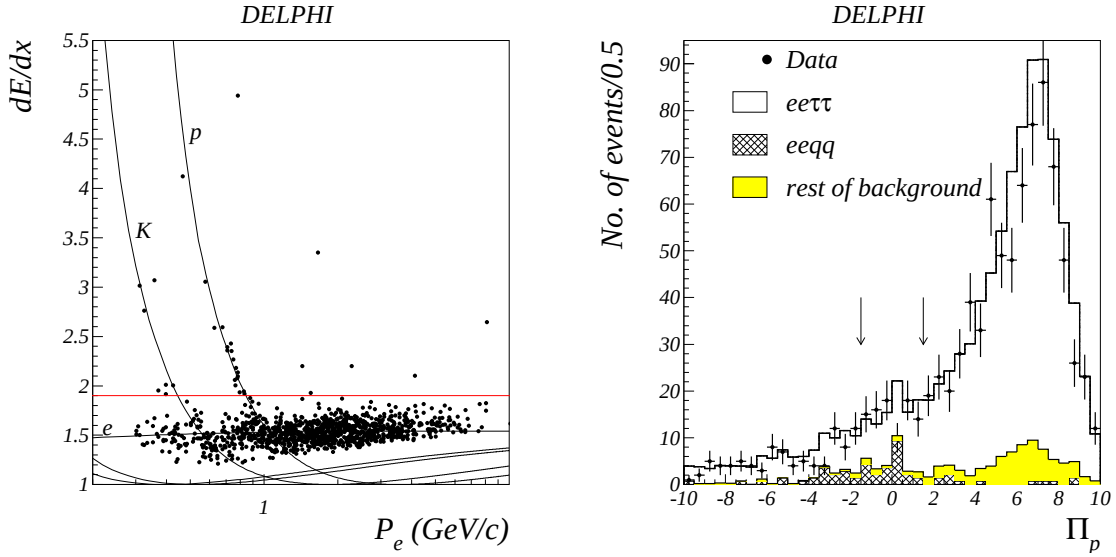

Figure 4: Left: specific energy loss as a function of particle momentum for electron candidates after preselection cuts and the cuts on the electron and muon pulls. The horizontal line shows the first cut against kaons and protons. The points are 1999 data. Right: distribution of *dE/dx* pull for proton hypothesis for electron candidates. The hatched histogram is the background from $e^+e^- \to e^+e^-q\bar{q}$ events and the shaded histogram is the rest of the background. The cuts against protons are indicated by arrows. All other selection cuts are applied. The points are 1999 data.

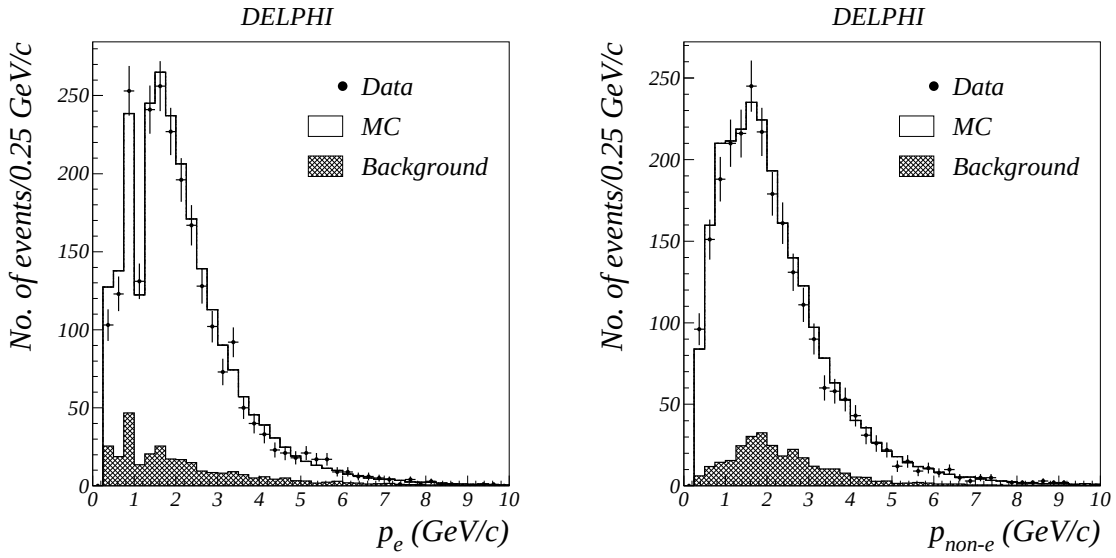

Figure 5: Momentum distribution for electron candidates (left) and non-electron candidates (right) for selected events from 1997-2000 data. The distributions of simulated events are corrected for trigger efficiency. The dip in the electron momentum distribution near 1 GeV/c is caused by the cut against protons: the electron and proton dE/dx are equal in this region of momentum.

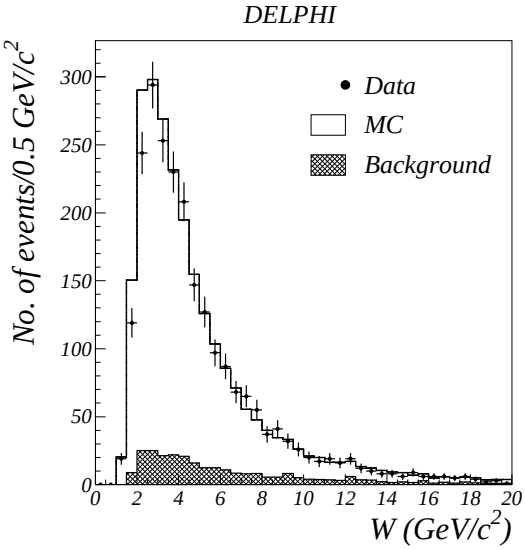

Figure 6: Visible invariant mass distribution for selected events for combined 1997-2000 data. The distribution of simulated events is corrected for trigger efficiency. The mass was calculated using all detected charged particles and photons. The simulation was corrected for the trigger efficiency.

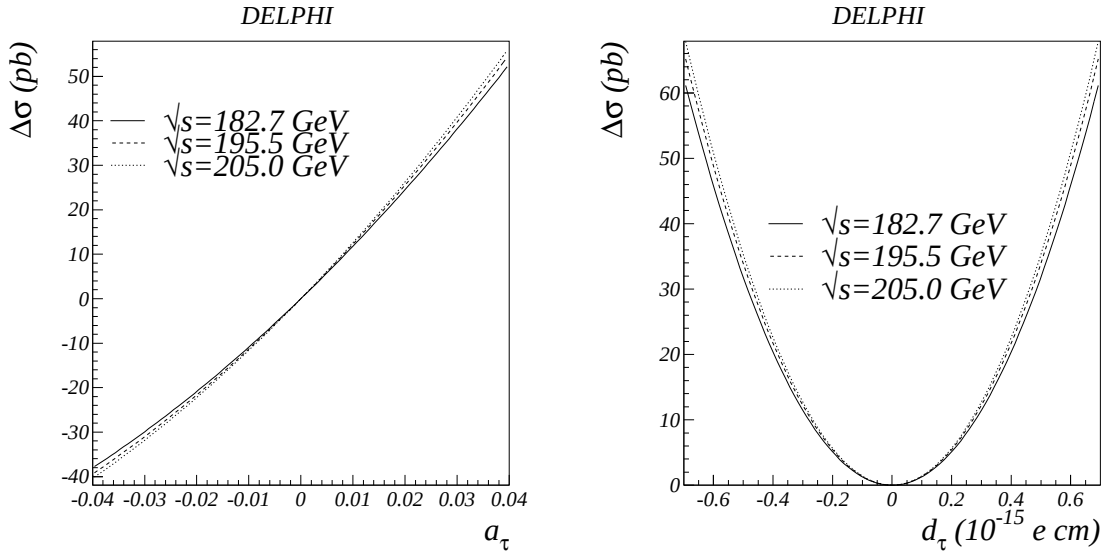

Figure 7: Total cross-section change as a function of anomalous magnetic moment and as a function of electric dipole moment.

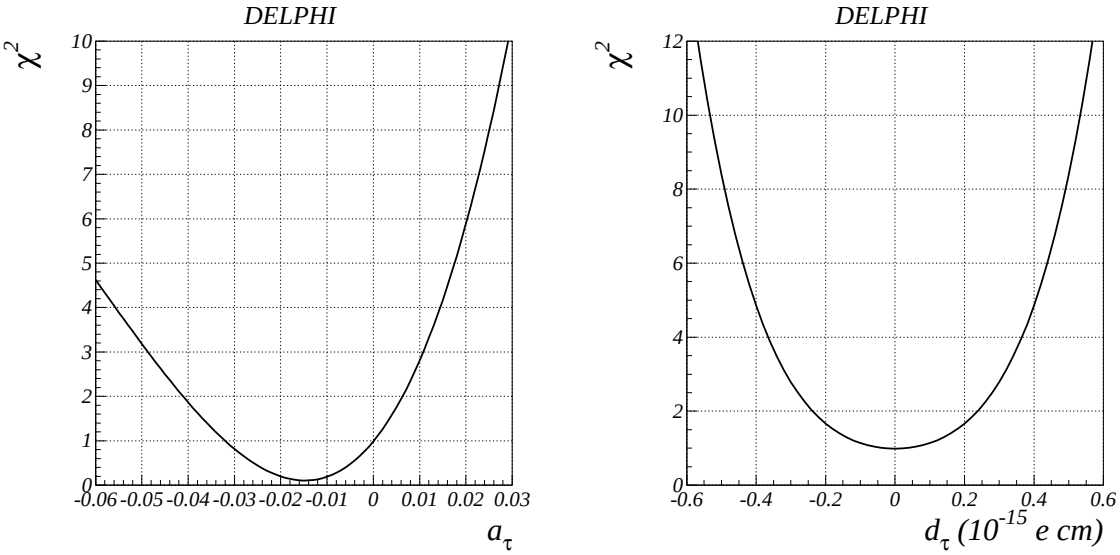

Figure 8: χ^2 as a function of anomalous magnetic moment and as a function of electric dipole moment.

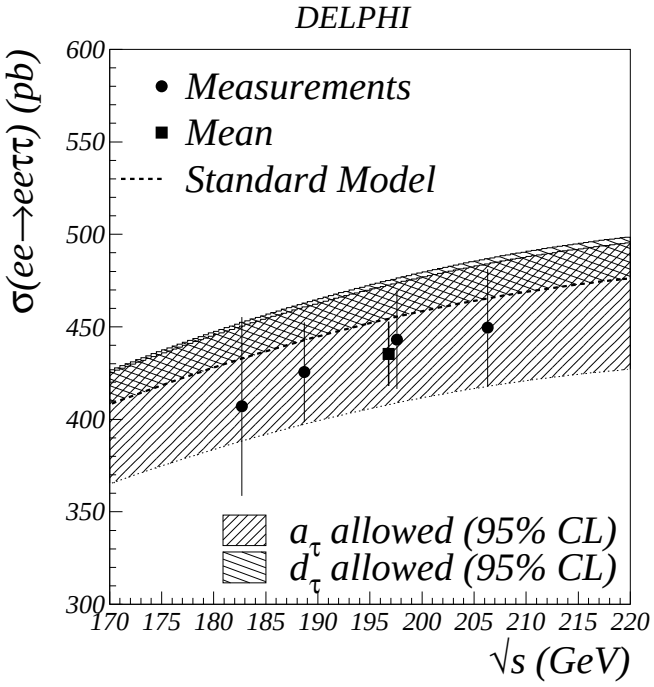

Figure 9: Measured cross-section (circles), average LEP2 cross-section (square) and SM expectation as a function of $\sqrt{s}$. The two bands show the cross-section variation allowed due to anomalous magnetic and electric dipole moments within 95% limits from this analysis.